Chapter 4

To synthesize pectin-iron complex from Assam lemon peel pectin, its characterization and iron bio-accessibility

4.1. Introduction

One of the major nutritional problems present globally is micronutrient malnutrition, especially iron deficiency, affecting millions of people, especially infants, children, and pregnant women. Mostly, iron deficiency is prevalent in school-aged children in developing countries. The deficiency of the same induces anaemia, increased susceptibility to infection, and decreased cognitive abilities and motor activity among individuals (Kinyoki et al., 2021). The World Health Organization (WHO) has proposed three approaches to combat micronutrient malnutrition such as food diversification and education, fortification, and supplementation (World Health Organization, 2006). However, if taken orally, Fe supplements could result in multiple gastrointestinal side effects due to the release of free Fe ions (Ma et al., 2021). Hence, alternative Fe supplements with limited or no side effects are highly desirable.

A study reported the effectiveness of a complex formed between a polysaccharide and Fe(III) as an oral Fe supplement. This complex demonstrated favourable characteristics such as water stability, chemical solubility, and minimal side effects (Saini et al., 2014). However, there are certain issues linked with the utilization of polysaccharide-Fe(III) complexes, such as the acidic pH in gastric fluid during the process of Fe digestion can lead to the degradation of the composition of a few polysaccharide-Fe(III) complexes, causing the release and dissolution of Fe ions (Cheng et al., 2019). Additionally, insoluble ferric compounds may develop in the intestinal juice, which may not be absorbed by the small intestine (Wang et al., 2015a). Therefore, the main challenge for polysaccharide-based carriers lies in retaining Fe ions in the presence of gastric juice. Pectin, a substance with excellent gelling properties against gastric acid, is considered a promising solution (Khramova et al., 2019). Importantly, pectin does not degrade when exposed to digestive enzymes present in the small intestine (Ma et al., 2021). Consequently, employing pectin to transport Fe ions seems to be a logical approach.

Pectin is a type of anionic polysaccharide which primarily contains D-galacturonic acid residues linked together through α-(1→4)-glycosidic bonds, along with different neutral sugar residues. Pectin has gained much significance globally due to its diverse range of bioactivities and effectiveness. Additionally, it has shown promise in biomedical research for drug delivery, antioxidative effects, and promoting wound healing. Pectin also significantly lowers blood cholesterol among patients. A patient must consume at least 6 g

of pectin each day for their cholesterol to be significantly reduced (Abdulhakeem et al., 2023). Pectin has several advantages when added to food and drug formulations (Moslemi, 2021). One of them is the presence of divalent cations in pectin results in the formation of stable gels, making them suitable carriers for delivering bioactive substances (Tyagi et al., 2015) and actively managing obesity and weight loss issues (Abdulhakeem et al., 2023). Pectin from the varying sources has been reported to be effective in health management, like lowering cholesterol, which lowers cardiovascular-related risks (Naqash et al., 2017). Another reason is pectin has been regarded as harmless, easily accessible, and having low production costs (Abdulhakeem et al., 2023).

Hence, this objective aims to create a citrus-based pectin-iron complex (PIC) to develop a novel Fe supplement. This involves complexing ferric ions with citrus pectin. The resultant complex was characterized using Spectrometric techniques, Scanning Electron Microscopy (SEM), Degree of esterification (DE), and galacturonic acid analysis. Moreover, the absorption of Fe from synthesized PIC was studied through in vitro assays and the Caco-2 cell model.

4.2. Materials and Methods

4.2.1. Raw materials and chemicals

The freshly harvested lemon samples were collected from the Citrus Garden, Tezpur University, Assam, India, during the period of June-July, 2021. The lemons were washed, peeled and subjected to tray drying at 45°C/10 h and finely powdered. The lemon peel powder was then sifted via a sieve (40-mesh) and stored at ambient temperature. Caco-2 cells (P-35) were supplied by Prof. Lisa Connolly, School of Biological Sciences, Queen's University Belfast, UK. Pepsin sourced from porcine gastric mucosa ≥2500 units/mg protein (P7012), pancreatin sourced from porcine pancreas (P7545, 8X USP), and bile extract porcine (B8631) were purchased from Sigma-Aldrich (Dorset, UK). The rest of the reagents were analytical grade purchased from Sigma-Aldrich (Dorset, UK).

4.2.2. Pectin extraction and its purification

Citrus pectin from Assam lemon peels was separated using the conventional method as described in section 3.2.3.1.). Briefly, 5 g dried peel powder was suspended in 150 mL of citric acid solution (pH 2). The solution was heated at 90°C using a water bath shaker for

60 min and cooled down to room temperature (RT). It was filtered using a cheesecloth to separate any solid particles. The resulting crude pectin filtrate was collected and then subjected to precipitation with ethanol (99%) in a 1:2 (v/v) ratio undisturbed at RT/3 h. Following this, the precipitated pectin underwent centrifugation (6500 rpm/15 min/room temperature), separating the wet pectin fraction. Following that, the wet pectin fraction underwent a washing process twice with 150 mL of ethanol to eliminate any remaining monosaccharides and disaccharides. The acquired moist pectin was dried at 40°C in a hot air oven until constant weight was achieved. The obtained dried pectin was finely powdered using a mortar pestle and preserved in a sealed container at RT for further use.

4.2.3. Formulation and experimental design of the PIC

The pectin extracted from Assam lemon peels (refer to section 4.2.2.) was complexed with Fe by modifying the method mentioned in Chirug et al. (2018). Based on the preliminary results, the pectin (0.5% w/v) was suspended in the iron III chloride hexahydrate ($FeCl_3.6H_2O$), in a concentration ranging from 0.90 mM to 1.80 mM for 180 h at RT. After incubation, the solution was subjected to centrifugation at 6000 rpm for 10 min to eliminate unbound Fe from PIC. The PIC was dialysed in de-ionized water for 48 h/RT, freeze-dried (6 h) and then transferred to a sealed container at RT for further analysis.

The formulation of PIC was modelled and optimized using a three-level of one-factor response surface methodology design (7 experimental runs). The details of the experimental design have been mentioned in Table 4.1. The parameters of the process and their corresponding range were selected according to initial observations aimed at examining their influence on the response variable, Fe content (ppm) within the PIC. The general linear equation involving process variables was presented in the Equation 4.1.

$$Y = \beta_o + \beta_1 x_1 + \beta_2 x_2 \ldots\ldots + \beta_k x_k \quad (4.1)$$

Where, Y is the response variable, β_o is the intercept term, β_1, β_2, and β_k represent the coefficient associated with the independent variables, and x_1, x_2, and x_k represent levels of the independent variables considered in the study (Eberly, 2007). All experimental runs were done in triplicates. The effect of independent variables was analysed by employing Design Expert (Version 12) to do regression analysis and ANOVA test. The level of significance was analysed on the basis of the F-value at a 95% confidence interval.

Table 4.1. The one-factor design for the optimization of iron content in pectin-iron complex PIC

Run	Iron chloride (mM)	Iron concentration in PIC (ppm)
1	1.35	2217.24
2	1.80	3776.74
3	1.13	2360.51
4	0.90	1238.41
5	1.80	3672.78
6	0.90	1538.25
7	1.58	2821.32

4.2.4. Determination of Fe content in PIC

The Fe content in PIC was measured by ICP-OES (inductively coupled plasma optical emission spectrophotometry) (Model: 5100 ICP-OES, Make: Agilent Technologies, USA). The PIC powder (0.1 g) was taken in labelled 50 mL centrifuge tubes, and 2 mL nitric acid (69%) was added to all tubes. After incubating the tubes overnight at RT, 2 mL of hydrogen peroxide was added to the respective tubes, and they were allowed to release gas for 15 min in a Class II safety cabinet. The tubes were then placed in a microwave digestor's carousel, and a digestion program consisting of three stages was initiated, which could take a total of 65 min, including the cooling process. The chosen program gradually heated the samples for 35 min, reaching a temperature of 95°C followed by 30 min digestion. The heating stages were as follows: a 5-min ramp from RT to 55°C, a 10-min hold at 55°C, a 5-min ramp to 75°C, a 10-min hold at 75°C, a final 5-min ramp to 95°C, and a 30-min hold at 95°C. Subsequently, the volumes were adjusted to the final weight of approximately 30 g using deionized water, and the precise masses were recorded. The iron (Fe) content in PIC was then run into ICP-OES. The determination was conducted in triplicates (Wahengbam et al., 2019).

4.2.5. Physicochemical properties of PIC

4.2.5.1. Determination of degree of esterification (DE)

The FTIR analysis method was used to determine DE. The term DE denotes the proportion of carboxyl groups (COOH) that have undergone methylation compared to the total COOH in a molecule. The DE (%) was calculated according to Equation 4.2 (Liew et al., 2016a):

$$DE(\%) = \frac{A_{1745}}{A_{1745}+A_{1630}} \times 100 \quad (4.2)$$

where, A_{1745} and A_{1630} represent the absorbance intensity at wavelengths 1745 cm^{-1} and 1630 cm^{-1}, respectively.

4.2.5.2. Galacturonic acid

The galacturonic acid content in the PIC was analysed using the 3,5-dimethyl phenol method described by Kumar and Kumar (2017). In a test tube, 0.25 mL PIC solution (1 mg/mL in distilled water) was mixed with 0.25 mL of sodium chloride solution (2% w/v) and 4 mL of concentrated sulfuric acid (37% w/v). The solution was then heated at 70°C for 10 min, followed by cooling it to RT. Then, 0.1 mL of a 3,5-dimethyl phenol solution (10 mg of 3,5-dimethyl phenol in 10 mL glacial acetic acid) was added and mixed. Immediately afterwards, the absorbance difference at 450 nm and 400 nm was measured using a UV-Vis spectrophotometer. D-galacturonic acid solutions (0.2-2 mg/mL) were used as a reference standard for the calibration curve. The galacturonic acid content of the PIC was calculated using this calibration curve. The absorbance difference of the standard was multiplied by a correction factor of 1.1.

4.2.5.3. Methoxyl group content

The methoxyl group content of pectin and PIC was determined using the method of Ranganna (1995) by Equation 4.3.

$$Methoxyl\ group\ content\ (\%) = \frac{Volume\ of\ alkali\ (mL) \times Normality\ of\ alkali \times 3.1}{Weight\ of\ sample\ (g)} \quad (4.3)$$

4.2.5.4. Molecular weight estimation

The molecular weight estimation of PIC and pectin was done using Gel Permeation Chromatography (GPC). For GPC analysis, the pectin sample was dissolved in distilled water to prepare a solution with a 1 mg/mL concentration. The solvent flow rate was 1 mL/minute. The mobile phase included a buffer solution with 0.2 M sodium nitrate ($NaNO_3$) and 0.01 M sodium dihydrogen phosphate (NaH_2PO_4). The GPC system (Agilent 1260 Infinity II) was equipped with two PL-aquagel OH Mixed-H columns (dimensions: 300 mm × 7.5 mm, 8 µm particle size) connected in series and a guard column of the same type. The instrument was coupled with a Refractive Index Detector (RID), maintained at a temperature of 35°C. Polyethylene glycol (PEG) and polyethylene oxide (PEO) standards were used to calibrate the system. The molecular weight distribution and parameters, including number-average molecular weight (Mn), weight-average molecular weight (Mw), and polydispersity index (PDI), were calculated based on the calibration curve constructed using the PEG and PEO standards. The data was processed using the Agilent Technologies GPC/SEC software.

4.2.6. Structural properties of PIC

4.2.6.1. Fourier transform infrared (FTIR) analysis

About 1 mg of PIC was mixed with 10 mg of potassium bromate and subjected to hydraulic pressing to form a pellet. Subsequently, the scanning of the pellet was done using an FTIR spectrophotometer (Model: Nicolet Instruments 410 FTIR, Make: Thermo Scientific, USA) across the frequency (400-4000 cm^{-1}) with a resolution of 4 cm^{-1} (Ma et al., 2021).

4.2.6.2. X-ray diffraction (XRD) analysis

The PIC's crystal structures and atomic spacing were examined using XRD study. The diffraction patterns of crystals of the PIC were recorded using an XRD instrument (AXS SMART APEX-I, Bruker, Germany). The radiation settings were maintained at 40 kV and 40 mA. The scanning range extended from 2θ of 5° to 80°, and the scanning rate was set at 4 degrees per min (Mundlia et al., 2019).

4.2.6.3. Scanning electron microscopy (SEM)

Images of the PIC were taken following the application of gold sputter coating to carry out the evaluation of the surface morphology of the PIC, particularly focusing on single crystals. This investigation was conducted utilizing a dual-beam Focused Ion Beam (FIB) TESCAN LYRA3 instrument (Wang et al., 2020). SEM image of pectin and PIC was captured at a view field from 1.38-3.85 mm with a scale bar indicating a length of 200 µm-1mm and in 75x to 200x magnification range.

4.2.7. Rheological study of PIC

4.2.7.1. Preparation of pectin and PIC solutions

Pectin and PIC solutions were prepared to study their flow behaviour properties at different concentrations. 1, 2, and 3% (w/v) of pectin/PIC were dissolved in distilled water at 80°C until completely dissolved. 30% (w/v) of sucrose was added for stable gel formation and mixed thoroughly to the respective solutions. After the complete dissolution of sucrose, 2.25% (w/v) $CaCl_2$ was added to ensure to make up the required concentration of 50 mg Ca^{2+}/g pectin/PIC. Finally, the resulting gels were boiled for 1 min under continuous stirring and stored at 4°C overnight before analysis (Jong et al., 2023). Based on suggestions from earlier research (Han et al., 2017; Yapo and Koffi, 2006), a set concentration of calcium (50 mg Ca^{2+}/g pectin) and sucrose (30% w/v) was used for pectin gel preparation in order to support stable gel formation.

4.2.7.2. Flow behaviour analysis

The rheometer (MCR72, Anton Paar, Austria) is equipped with cone and plane geometry (40 mm, 1° angle and 0.5 mm gap). The steady flow behaviour of the prepared pectin/PIC solutions was measured at a shear rate ranging between 0.1 – 100 s^{-1} at a constant temperature of 25°C. The viscosity (Pa.s) was tested as a function of the shear rate (s^{-1}). The data obtained were fitted to different flow equations (Newtonian, power law, and Herschel–Bulkley) to find the best-fitting model.

4.2.7.3. Viscoelastic properties analysis

Pectin and PIC powder were dissolved in distilled water to prepare pectin and PIC solutions with a 1%, 2%, and 3% (w/v) concentration. The rheometer (MCR72, Anton Paar, Austria) equipped with parallel plate geometry (60 mm diameter) and a 1 mm gap between plates was used to conduct dynamic frequency sweeps. The strain (1%) was kept within the linear viscoelastic zone during tests, which were performed at a constant temperature of 25°C over an angular frequency range of 0.1 to 100 rad/s producing storage modulus (G′) and loss modulus (G″).

4.2.8. Thermal study of PIC

4.2.8.1. Differential Scanning Colorimetry

The thermal characteristics of the pectin and PIC in a nitrogen environment were measured using a differential scanning calorimeter (DSC 214 Polyma, Netzsch, Germany). A sample of around 10 mg was weighed and sealed with the lid inverted in an aluminium concave pan. A blank sample was used as a control. The samples were heated from 30-300°C at a rate of 10°C/min. The enthalpy (H), conclusion temperature (Tc), peak temperature (Tp), and onset temperature (To) were obtained from the thermogram.

4.2.8.2. Thermogravimetric analysis

The degrading parameters of pectin and PIC were examined using thermogravimetric (TGA) processing. A thermogravimetric analyzer (TG 209 F1 Libra, Netzsch, Germany) was employed to evaluate each sample's thermal stability. Samples were heated at a rate of 10°C/min to temperatures between 25°C and 600°C in a nitrogen environment.

4.2.9. *In vitro* Fe release from PIC for assessment of bioaccessible Fe

Bioaccessibility of Fe in the pectin and PIC was carried out using the INFOGEST *in vitro* digestion protocol (Brodkorb et al., 2019). In order to replicate the human digestive system, *in-vitro* digestion was performed, which consisted of three main steps: oral, gastric, and intestinal digestion. In the oral phase, 1 g of PIC powder was combined with a 30 mL solution containing 140 mM NaCl and 5 mM KCl in a 1:1 (v:v) ratio. Then, 25 µL CaCl2 (0.3M) and 500 µL of 100 mM ascorbic acid solution were added to the oral

bolus. The oral bolus was placed in a water bath shaker at a rate of 200 rpm maintained at 37°C for 2 min. For the gastric phase, 0.5 mL of pepsin solution with an 11000 U/mL concentration was introduced to the previously orally digested sample. The pH of 3 was adjusted using 1 M HCl. The oral bolus was thereafter placed in a shaking water bath for 2 h at 200 rpm and 37°C. The gastric chime was adjusted to pH 5 after incubation using 1 M NaHCO3 for the intestinal phase. Following pH adjustment, a 2.5 mL solution of the pancreatin-bile mixture (0.45 g bile salts and 0.075 g pancreatin in 37.5 mL of 0.1 M $NaHCO_3$) was introduced to the gastric chime. After adding 40 µL $CaCl_2$ (0.3 M), the pH was adjusted to 7.0 using 1 M NaOH. The mixture was then incubated for 2 h in a shaking water bath set at 37°C/200 rpm. Following incubation, the samples that had undergone digestion were cooled in ice for 10 min and centrifuged at 3500 g^{-1} for 1 h at the temperature of 4°C. The resulting supernatants (soluble mineral fraction) were carefully isolated and stored at −80°C for subsequent analysis.

4.2.10. Quantification of bioaccessible Fe

The supernatants from the preceding step (Section 4.2.7.) were analysed for bioaccessible Fe by ICP-OES (Section 4.2.4.). The % bioaccessibility of Fe in PIC was calculated by using Equation 4.4.

$$\%bioaccessibility = \frac{bioacessible\ m.f.}{total\ m.c.} \times 100 \quad (4.4)$$

where the bioaccessible mineral fraction (bioaccessible m.f.) and the total micronutrient content (m.c.) represent the soluble Fe fraction obtained post-simulated digestion and the overall Fe content found in dried PIC (ppm), respectively (Wahengbam et al., 2019).

4.2.11. Fe release study from PIC using Caco-2 cells

As mentioned in section 4.2.9, the soluble m.f. from the *in-vitro* simulated digestion was used to examine the bioavailability of Fe transfer across Caco-2 cells. The cells were cultured in flasks (75 cm^2) and nurtured in a nutrient medium comprising Dulbecco's minimum essential media (MEM). Fetal bovine serum (10% v/v), sodium pyruvate (1% v/v), 4 mM L-glutamine, and 1% (v/v) penicillin-streptomycin were added to the solution. The cells were incubated (5% CO_2 and 95% relative humidity) at 37°C under standard conditions (Wahengbam et al., 2019).

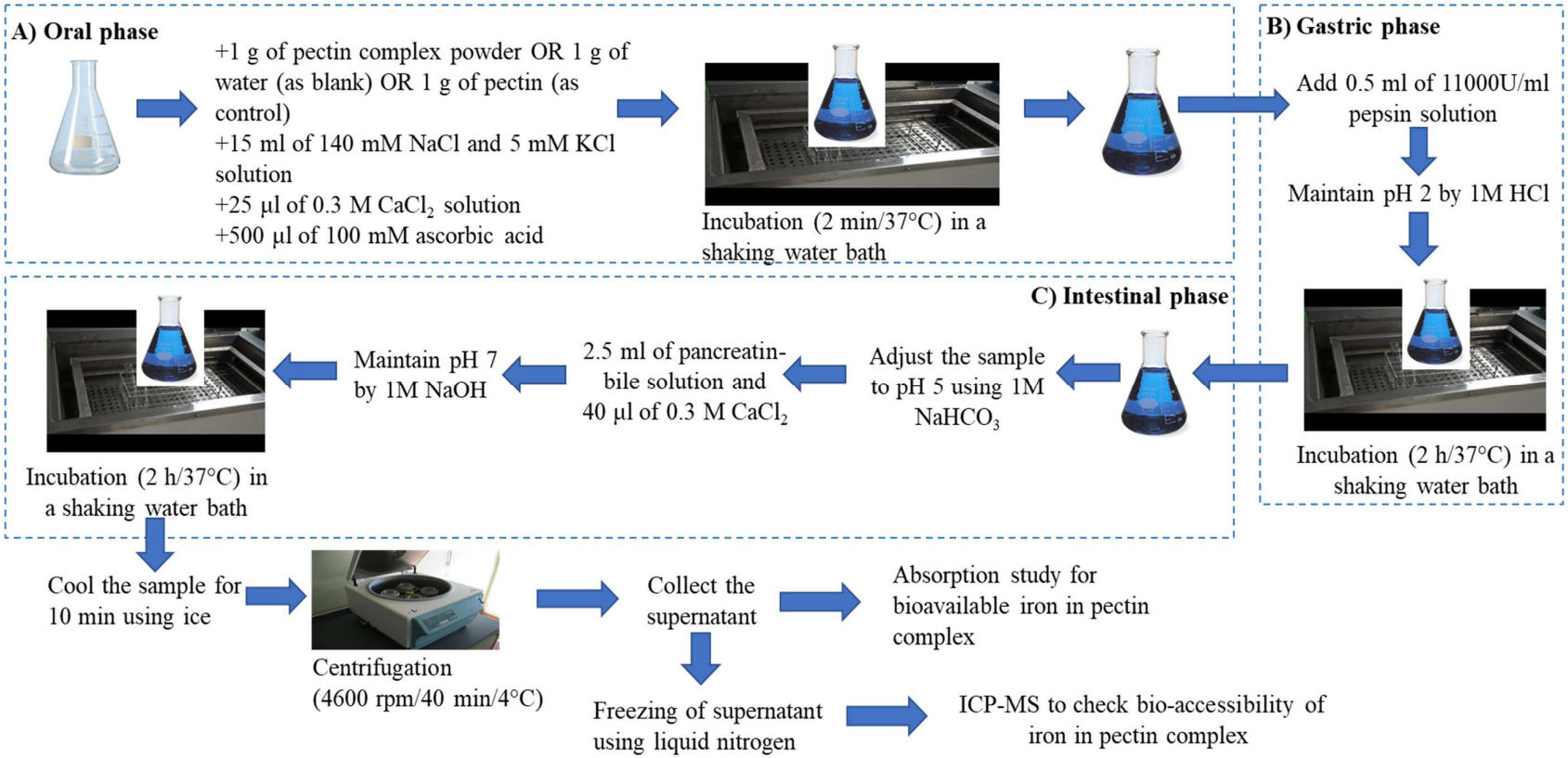

Figure 4.1. *In-vitro* digestibility of developed pectin complex methodology

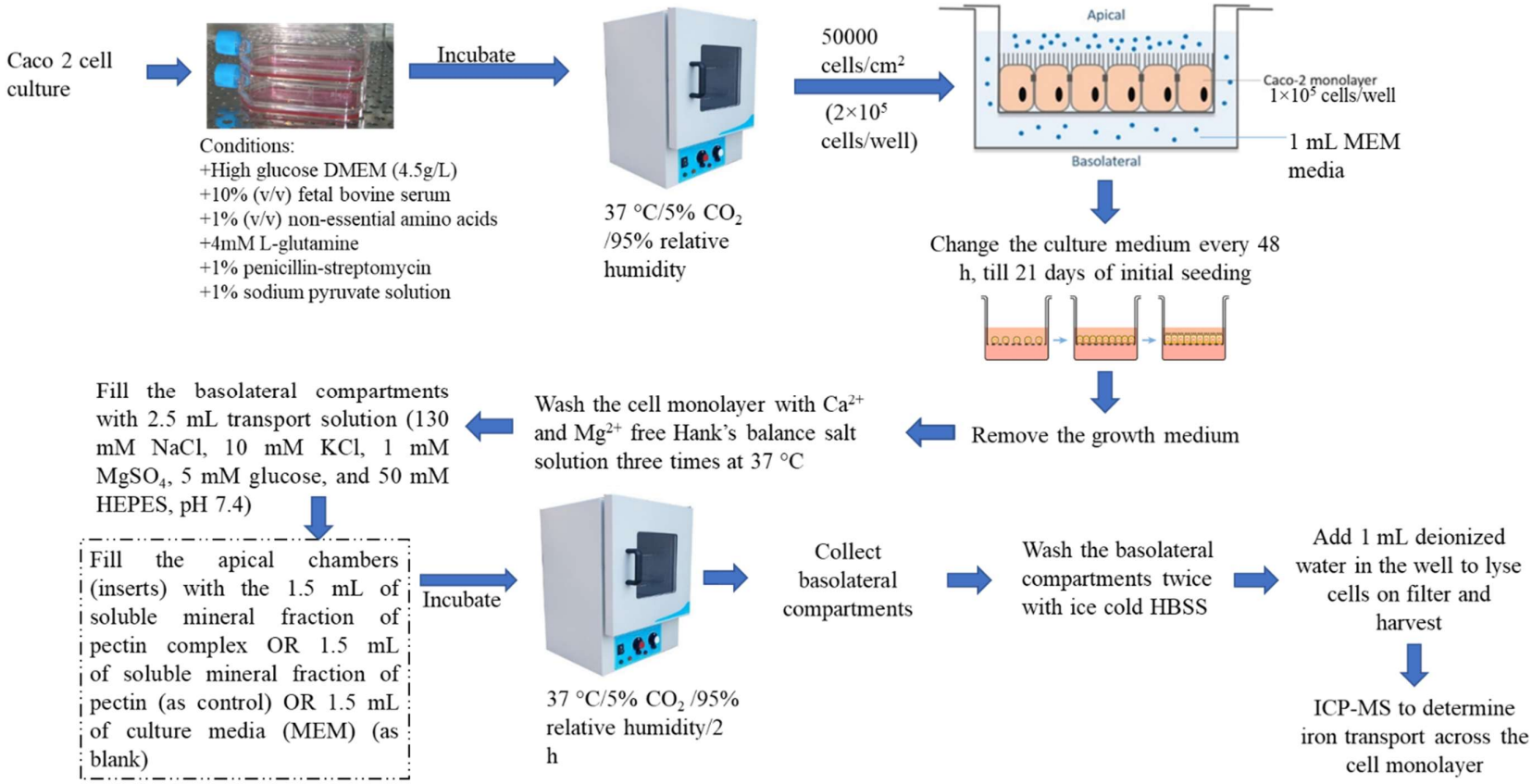

Figure 4.2. Absorption (transport) study for bioavailable iron through Caco-2 cells methodology

For testing the bioavailability, 0.1 mL of the cell solution, having 2×10^5 cells/well for each 6.5 mm diameter filter, was seeded in the inserts (apical compartment) of 24 well plates, while 0.6 mL of nutrient medium was added to the basolateral compartment. The plate was then incubated with the filter supports at 37°C in an incubator with 5% CO_2, and 95% relative humidity for 6 h. After incubation, the apical medium was removed without disturbing the inserts and replaced with 0.1 mL of nutrient medium to remove non-adherent cells, thus reducing the risk of multilayer formation. The nutrient medium was refreshed every 48 h during the initial 21-29 days after seeding. After this time frame, the growing media was removed. Then, 0.6 mL and 0.1 mL of Ca^{2+} and Mg^{2+} free Hank's balance salt solution (HBSS) were poured in the basolateral and apical compartments, respectively, to rinse the cell monolayer. Iron can compete with calcium and magnesium ions for binding sites on transport proteins and chelators. The competition for these binding sites is reduced by utilizing a Ca^{2+} and Mg^{2+} free solution, which results in more precise iron binding and absorption studies. After 20 min of incubation at 37°C and 100 rpm, the plates were removed, and the HBSS was poured out of both compartments. For the transport experiment, 0.6 mL of HBSS and 0.1 mL of soluble mineral fraction (section 4.2.9) were included in the basolateral and apical compartments, respectively. The plates were thereafter subjected to incubation at 37°C for 2 h at 500 rpm in an incubator shaker. The sample was obtained from the basolateral compartment and preserved at -80°C in order to assess the absorption of Fe and the transportation of bioavailable Fe across the cell monolayer using ICP-OES (section 4.2.4.). The viabilities of the cells were evaluated using trypan blue exclusion, with typical rates ranging between 92-97% following a 2-h exposure period.

$$\%\ absorption\ of\ bioavailable\ iron = \frac{Transport\ x_{basolateral}}{Bioaccessible\ x_{apical}} \times 100 \qquad (4.5)$$

where "transport $x_{basolateral}$" represents the quantity of Fe (ppm) that has been carried out via the cell monolayer to reach the basolateral compartment. On the other hand, "bioaccessible x_{apical}" in the apical compartment signifies the quantity of bioaccessible Fe (ppm) (Wahengbam et al., 2019).

4.2.12. Statistical analysis

Data analysis was performed using the one-way analysis of variance (ANOVA) method, and Duncan's mean comparison test was conducted at a significance ($p \leq 0.05$) to identify any variations among treatments. The statistical analysis was carried out utilizing IBM SPSS Statistics 20. The experiment is conducted in triplicates, and data is performed in mean ± standard deviation.

4.3. Results and Discussion

4.3.1. Formulation and optimization of PIC

Based on preliminary results, a one-factor design using Design Expert 12.0 version was designed keeping 180 h as the constant incubation time and iron chloride hexahydrate concentration ranging from 0.90 mM to 1.80 mM as an independent variable for optimizing PIC. The iron concentration (dependent variable) in PIC at different concentrations of iron chloride hexahydrate (independent variable) varied between 1238.41 to 3776.74 ppm. According to the I-optimal design, a linear model was evaluated. The analysis of variance (ANOVA) depicted the significance of the model variations compared to the variation of the experimental results. The results of the ANOVA are mentioned in Table 4.2. The linear model *F*-value of 70.34 implies the model is significant.

The R^2 and adjusted R^2 values for the obtained iron concentration were determined to be 0.9336 and 0.9204, respectively. These values indicate a strong correlation between the predicted and actual iron concentrations, with no significant difference noted between them. The coefficient of variation, assessing the relative dispersion of experimental data from the model predictions, was found to be 10.95%. This lower coefficient suggests minimal deviation between experimental and predicted values, highlighting the model's accuracy. Furthermore, the adequate precision, which gauges the signal-to-noise ratio, was calculated to be 14.793 for the iron concentration in PIC. This observation suggests that the model is capable of predicting data with higher accuracy. The linear equation, presented in coded form as Equation 4.6, includes significant parameters that contribute to the model's predictive capability.

$$I = +2517.89 + 1089.61*A \quad (4.6)$$

Table 4.2. The coefficients of linear equation and ANOVA test results indicating the effect of iron III chloride hexahydrate (mM) concentration on iron content in the pectin-iron complex (PIC)

Model Terms	
Intercept	+2517.89
Model- *Linear*	
A-Iron chloride hexahydrate concentration (mM)	+1089.61
Fit statistics	
R^2 model	0.9336
Adjusted R^2	0.9204
Model (F value)	70.34
Model (p value)	0.0004
Lack of Fit (F value)	4.36
Lack of Fit (*p value*)	0.1921 Not significant

In Equation 4.6, the parameter 'A' coefficient was determined to be 1089.61. The positive effect of the independent variable on a dependent variable indicates that an increase in the value of the independent variable (iron III chloride hexahydrate) increases the value of a dependent variable. So, the increase of iron chloride hexahydrate concentration increases the iron content in PIC. This might be due to a combination of factors related to the availability of iron ions and the binding capacity of pectin molecules. As the iron III chloride hexahydrate concentration increases, more iron ions are available in the solution (Persson, 2018). Maksudova et al. (2010) stated that this higher concentration provides more opportunities for iron ions to bind to the pectin molecules, increasing iron content in the PIC. Pectin molecules possess binding sites that can be complex with metal ions such as iron. However, they did not report the limiting concentration of iron. With a higher concentration of iron chloride hexahydrate, more iron ions are available to bind to these sites, resulting in an increased iron content in the PIC.

The linear equation presented in Equation 4.6 was utilized to determine the optimal conditions of process parameters aiming to achieve a target iron content of 3000 ppm in PIC. According to the model, an iron content of 2542 ppm was predicted at 1.36 mM of iron III chloride hexahydrate with a desirability of 1.000. Experiments were conducted at

the optimal conditions for validation, resulting in an observed iron content in PIC of 2657 ± 23.61 ppm. The relative deviation between the experimental and predicted response values under optimal conditions was 1.06%, indicating a good correlation between the predicted and observed values. This suggests that the developed linear model accurately predicts the iron content in PIC under the specified conditions.

4.3.2. Physicochemical properties of PIC in comparison with pectin

4.3.2.1. Proximate analysis

It was found that the moisture content of PIC (19.10 ± 1.12% w/w) and pectin (21.10 ± 1.43% w/w). Likewise, no statistical significance was found in the protein content of pectin (2.62 ± 0.21%) and PIC (2.34 ± 0.17%). On the other hand, Koh et al. (2014) reported that the protein and moisture contents of the pectin derived from jackfruit rinds were 1.53–1.74% and 5.19–9.98% w/w, respectively. Additionally, both PIC and pectin have no fat content. The ash content of pectin (2.785 ± 0.10%) was found to be lower than that of PIC (3.873 ± 0.10%).

4.3.2.2. Degree of Esterification (DE)

The term DE stands for the esterified COOH groups inside galacturonic acid chains with methyl or acetyl groups and is essential for determining the quality of pectin. On the basis of DE value, pectin is categorized as either high methoxyl (HM) pectin (DE ≥ 50%), or low methoxyl (LM) pectin (DE ≤ 50%) (Liew et al., 2016b). The DE values for the pectin (51.87%) and PIC (50.35%) exceed 50%, indicating that it falls into the category of HM pectin. This type of pectin is commonly used to produce jams and jellies.

4.3.2.3. Galacturonic acid

The concentration of galacturonic acid was higher than 65% for pectin and PIC however, pectin had higher galacturonic acid content (84.33 ± 1.44%) compared to PIC (67.39 ± 4.92%), which might be because pectin, after forming PIC, is not solely composed of galacturonic acid molecules. Due to the presence of negatively charged carboxylic groups, galacturonic acid exhibits a strong propensity to bind with Fe ions, forming a highly stable complex (Cheng et al., 2019).

4.3.2.4. Methoxyl group content

Methoxyl group content has a key role in regulating pectin's gel-forming ability and setting time. The methoxyl group content of pectin and PIC was found to be 2.02 ± 0.01% and 13.52 ± 0.04%, respectively. These results, however, were less than those reported for banana (7.03%) and mango (7.33%) peels (Apsara and Pushpalatha, 2002), but they were comparable to dragon fruit pectin (Zaidel et al., 2017), which had 2.98 to 4.34%. This could be due to the partial degradation of pectin. According to Aina et al. (2012), depending on the source and extraction conditions, pectin's methoxyl group concentration can range from 0.20 to 12%. The amount of methoxyl groups in fruits depends on their maturity because, as they mature, their sugar content rises while their methoxyl group content falls. A high amount of methoxyl groups improves pectin's capacity to bind sugar and its dispersion quality (Apsara and Pushpalatha, 2002).

4.3.2.5. Molecular weight of PIC

The weight-average molecular weight (Mw) of pectin and PIC was 296.748 kDa and 24.444 kDa, respectively. The Mw of PIC is less than pectin but in the general range of 8-1000 KDa for pectins from various fruit sources (Corredig et al., 2000; Wang et al., 2014). While, the number-average molecular weight (Mn) of pectin and PIC was 149.862 kDa and 14.326 kDa, respectively. After pectin complexation, the Mw and Mn of PIC decreased than compared to pectin. This might be because the PIC has lower galacturonic acid content and degree of esterification compared to pectin (Yang et al., 2023) as PIC is composed of iron ions and pectin molecules. Results of GPC showed that pectin had an additional low one peak while PIC had an additional low two peaks in the GPC profiles (data not shown). This indicates that pectin and PIC are composed of different molecular weight fragments.

The function of the polymer is significantly affected by the chain length of the polymer, thus it is necessary to study the molecular weight distributions of PIC. The polydispersity index (PD) of pectin (1.980) was decreased to that of PIC (1.706), exhibiting the effect of mineral complexation in pectin. In addition, the decrease in PD values in PIC indicates an increase in solution homogeneity (Chen et al., 2019). This could also be due to the loss of low molar mass molecules during the dialysis process of PIC (Lopes et al., 2017).

4.3.3. Structural characterization of PIC in comparison with pectin

4.3.3.1. Fourier Transform Infrared (FTIR) Spectroscopy

The FTIR spectra of PIC and extracted pectin are represented in Figure 4.3. The O-H stretching band (3100-3600 cm^{-1}), C-H stretching bands (2800-3000 cm^{-1}), and the fingerprint region (below 2000 cm^{-1}) were among the distinct distinctive sections that were the focus of the spectral investigation. Specifically, bands that contribute to the resonant absorption energy of the pyranose cycle vibrations (950-1200 cm^{-1}) and the area between 1200 and 1800 cm^{-1}, indicating the condition of carboxylic groups, were highlighted (Wang et al., 2014). Table 4.3 represents the FTIR frequency range and functional groups identified in the pectin and PIC. Hydrogen bonding and complexation inside the molecule determine the position of the C=O stretching wave number within these ranges. Delocalization of the C=O group following complexation with a C=C band causes the absorption to shift to a lower wave number (Stuart, 2004). Pectin and the PIC lacked lignin and proteins, as indicated by the absence of the bands at about 1600-1500 cm^{-1} that are attributed to aromatic rings and protein amide (Liu et al., 2019). The variations observed in the bands within specific regions, such as (C–H) bands at 2929 cm^{-1}, 1340 cm^{-1}, and 1240 cm^{-1}, as well as the complex band (C–H) spanning 1000-700 cm^{-1}, were attributed to alterations in the interactions between pectin and Fe (III). Furthermore, in the 1153-1019 cm^{-1} region, both the spectra of pectin and the PIC exhibited several highly fused bands. These changes likely reflect the complex interplay and molecular interactions between pectin and Fe (III) in the synthesized PIC. The loss of these bands may suggest that following Fe (III) chelation, changes occurred to the pectin's organized structures and glycosidic bridge (Wang et al., 2015a).

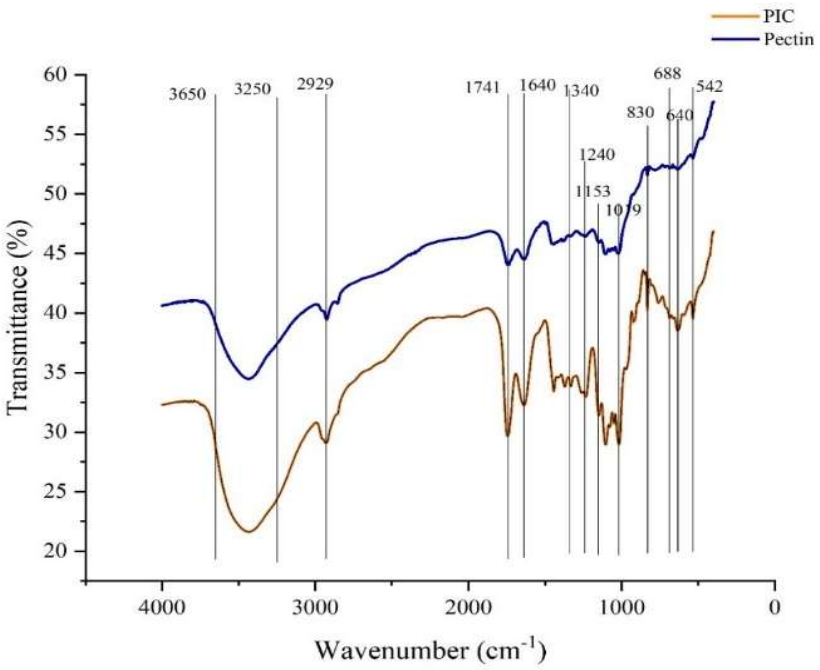

Figure 4.3. FTIR of pectin and PIC

Table 4.3. FTIR frequency range and functional groups present in the pectin and PIC

S.No	FTIR peak	Functional group assigned	References
1	3650-3250 cm^{-1}	O-H stretching of CH-OH groups from polysaccharide units O-H vibration of Iron (III) oxide-hydroxide (FeOOH) in iron hydroxide	Liang et al., 2012
2	2929 cm^{-1}	Inter- and intramolecular hydrogen of the C-H bonds of the CH2 and CH3 groups	Hosseini et al., 2016
3	1640 and 1741 cm^{-1}	C=O stretching vibration of carboxyl groups and esterified carboxyl moieties	Ognyanov et al., 2020

4	1010–1100 cm^{-1}	presence of furanoses and pyranoses, attributed to the tensile vibration of C–C, C–OH, and C–O–C bonds	Qi et al., 2023
5	1016–1019 cm^{-1}	Pectic compounds	Wang et al., 2014
6	830, 688, 640, and 542 cm^{-1},	FeOOH group structure in the fabricated complex	Wang et al., 2015a; Cui et al., 2018
7	400 cm^{-1} and 650 cm^{-1}	Fe–O band in PIC	Noqta et al., 2020

4.3.3.2. X-Ray diffraction (XRD)

XRD is a valuable technique utilized to study the amorphous or crystalline nature of pectin and analyse its physical and functional characteristics. In Figure 4.4, the XRD graphs depict the extracted pectin and the developed PIC. The diffraction patterns of the pectin exhibited a single peak around 2θ of 9.4°. However, new diffraction patterns emerged upon complexing pectin with ferric ions, revealing two peaks around 2θ of 6.15° and 10.65° (as shown in Figure 4.4.). These alterations in the diffraction patterns suggest changes in the crystalline or amorphous properties of pectin induced by the complexation process with ferric ions. The diffraction peak of PIC was sharper and more intense than pectin, resulting in larger crystallite grain size. The broad peaks of pectin disappeared after the coordination reaction, indicating a change in the crystal morphology. Similar results were observed in the soybean polysaccharide-iron (III) complex by Gao et al. (2018). The observed higher intensity of pectin compared to the PIC suggests a higher degree of crystallinity in pectin. The lower intensity of esterified C=O related peaks in the FT-IR spectrum of pectin implies a correlation between the crystallinity of pectin and its degree of esterification. Jiang et al. (2019) also noted that pectin with a higher degree of esterification tends to exhibit a higher degree of crystallinity. The crystallization process is attributed to hydrophobic interactions among methyl ester groups during the dehydration of pectin.

The evolution of the diffraction pattern indicates that the PIC is relatively more amorphous compared to pectin, despite having a higher crystallite grain size. This suggests that the

complexation with ferric ions influences the crystalline structure of pectin, potentially altering its physical properties and functionality. Therefore, PIC can be used as a gelling agent, thickener, and stabilizer in food products such as jams, jellies, fruit preserves, and confectionery.

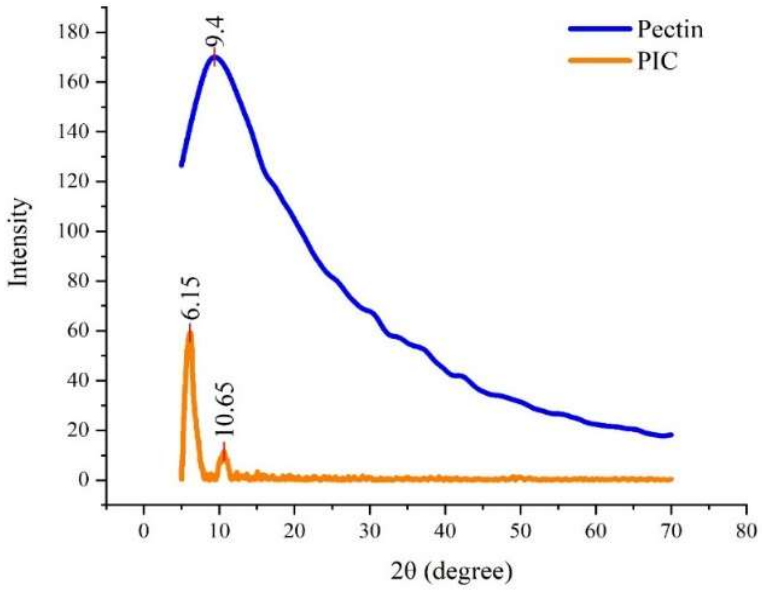

Figure 4.4. XRD of pectin and PIC

4.3.3.3. Scanning Electron Microscopy (SEM)

Surface morphologies of extracted pectin and developed PIC are illustrated in Figure 4.5. The overall texture of PIC appears relatively smooth and flat surface texture to that of pectin. This might be due to the coordination bonding between pectin and iron. Grains of PIC are visible, ranging in size from approximately 1.08 to 1.59 mm, and are relatively well-defined than that of pectin. Decreasing the view field to 2 mm from 3.85 mm reveals finer details within individual grains. The observed grain in PIC appeared to be cylindrical, while the pectin grain appeared to be a rock-like structure. Overall, SEM micrographs signify that PIC exhibited more disordered structures or less well-defined crystal lattices along with large grain sizes, which is in agreement with the diffraction patterns of PIC in XRD.

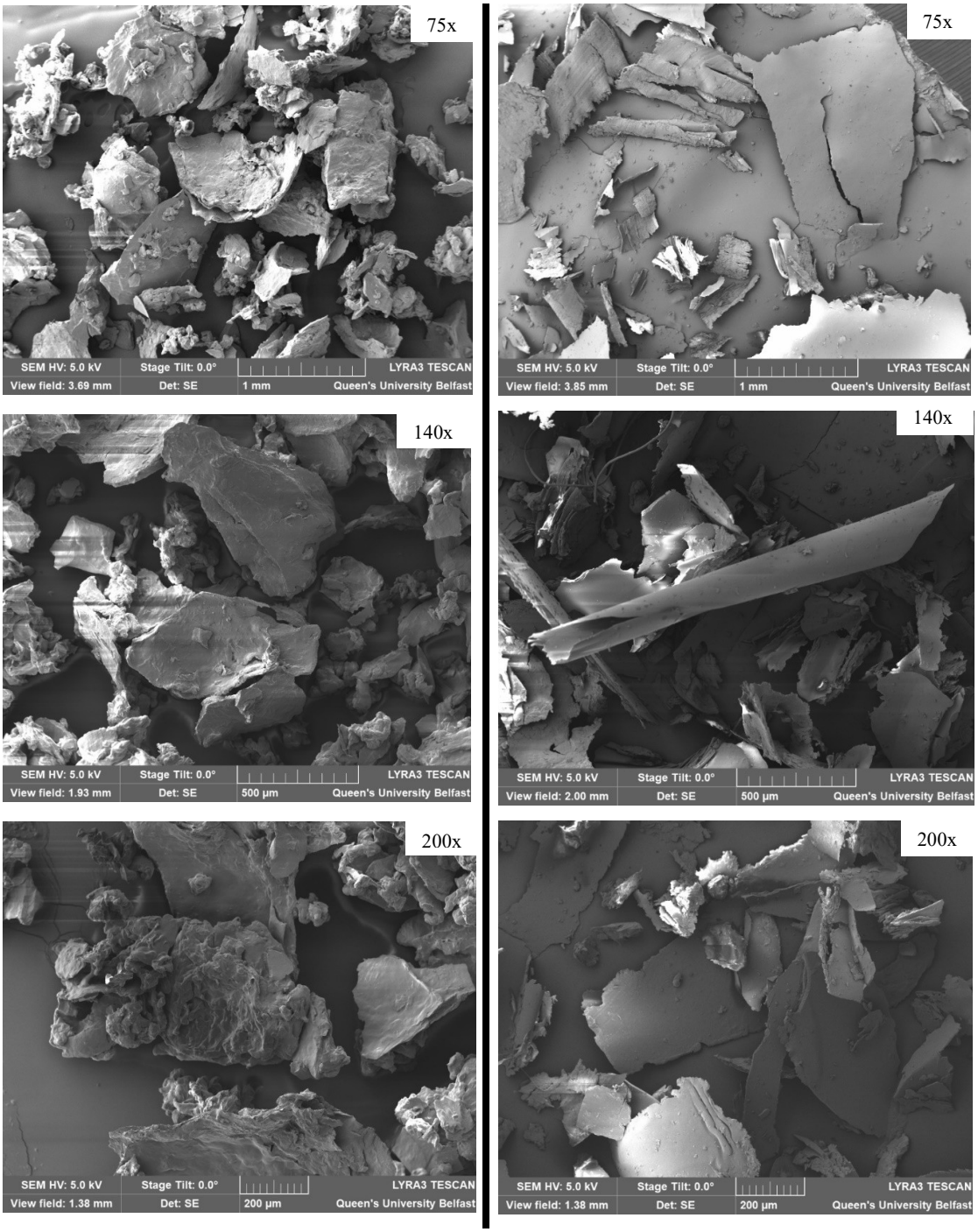

a) b)

Figure 4.5. SEM micrographs of a) pectin and b) PIC at different view fields

4.3.4. Rheological analysis of PIC in comparison with pectin

4.3.4.1. Flow behaviour

The flow behaviour of pectin and PIC solutions at various concentrations (1-3%) between 0-100 s^{-1} shear rate at 25°C is shown in Figure 4.6. With the increase in the shear rate, the viscosity of both pectin and PIC solutions decreased, resulting in shear thinning or pseudoplastic behaviour. The shear-thinning behavior may result from the orientation effect, wherein elongated molecule chains align with the direction of heightened shear rate. This breaks intermolecular bonds, leading to Newtonian fluid behavior in the pectin/PIC solution (Hua et al., 2015a). The pseudoplastic region of the solution is more pronounced at elevated concentrations compared to lower values, attributable to the increased intermolecular networks established among the pectin chains. Numerous studies have reported similar pectin flow behaviour (Li et al., 2023; Hua et al., 2015a; Colodel et al., 2019; Qin et al., 2020; Xiao et al., 2021). Pseudoplastic properties of such solutions make it easier to pump liquid food and provide a pleasing mouthfeel and body, making it suitable for culinary applications.

The viscosity of pectin/PIC solutions of 1-3% (w/v) concentrations at 50 s^{-1} shear rate is shown in Figure 4.7. This particular shear rate value was selected since it closely resembles the sensation felt in the oral cavity (Masson et al., 2011). From Figure 4.7, it can be seen that that the viscosity of the pectin solution increases as the concentration of pectin increases, which might be due to the decreasing intermolecular distances and increase in intermolecular interactions, including hydrogen bonds with the hydroxyl groups of pectin among pectin molecules. The presence of hydrated pectin molecules at higher concentrations leads to disruption in the velocity pattern of liquid (Liu et al., 2022). Hua et al. (2015a) and Colodel et al. (2019) also reported a similar trend. It can also be deduced from Figure 4.7 that the viscosity of the pectin solution was significantly higher than that of PIC, which could be due to the higher molecular weight of pectin (Mw =296.748 kDa). Since the longer galacturonan chain created more efficient junctions per chain, molecular interactions between pectin at a higher molecular weight increased (da Silva and Rao, 2006; Begum et al., 2021). Furthermore, when pectin chains are hydrated, their hydrodynamic size increases more due to higher Mw, which enhances viscosity (Hua et al., 2015a). Moreover, the pectin gel structure may be strengthened by dispersing agents, such as sucrose, in pectin (Fu and Rao, 2001).

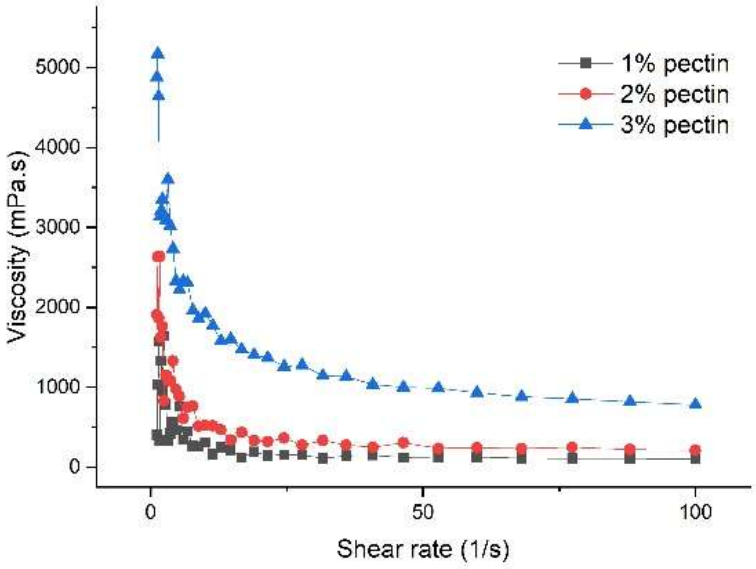

(a)

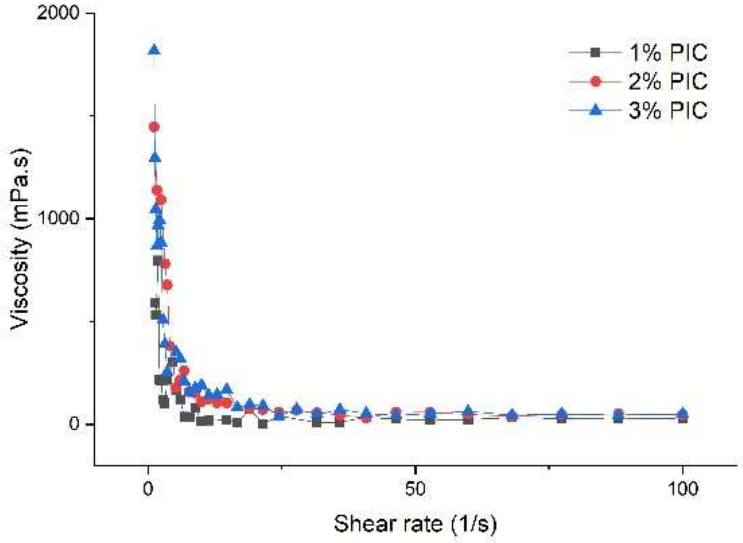

(b)

Figure 4.6 Viscosity-shear rate profiles of (a) pectin and (b) PIC solutions at concentrations 1.0–3.0% (w/v)

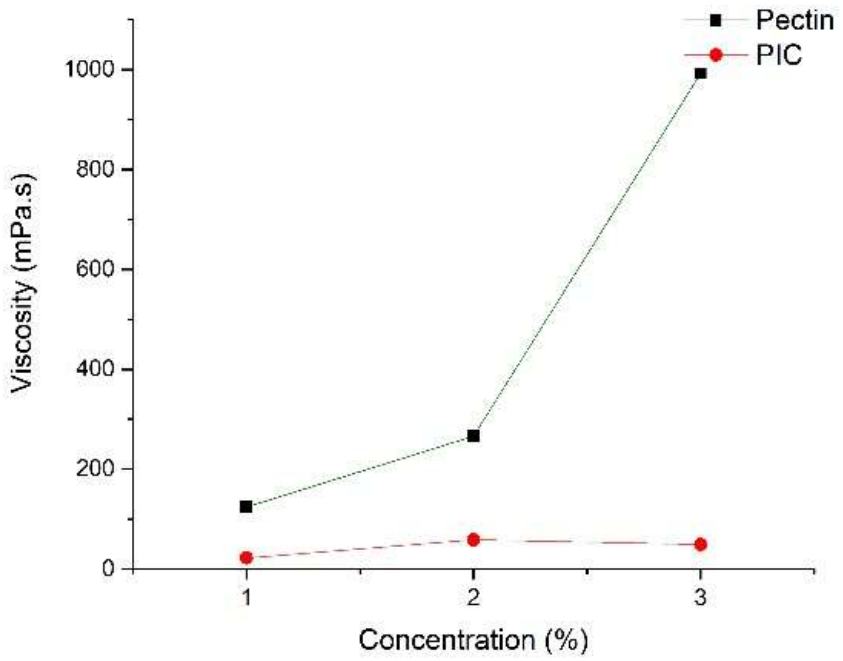

Figure 4.7. Effect of concentration on the viscosities of pectin and PIC solutions (shear rate = 50 s^{-1})

4.3.4.2. Modelling rheological behaviour

The rheological behaviour of pectin/PIC was fitted to three models (Power law, Newtonian and Herschel-Bulkley model) that helped in achieving the parameters such as consistency index (K) and flow behaviour index (n) to study the rheological behaviour of pectin/PIC. The results of the analysis are mentioned in Table 4.4. The flow measurement data was fitted to the Newtonian law model, and it can be seen from Table 4.4 that with an increase in the concentration of pectin/PIC solution, μ (viscosity in Newtonian liquid) is also increasing, which might be due to the presence of dense molecular network at higher concentrations. The pectin solution is more viscous as values of μ for pectin are higher than PIC at equivalent concentration. Moreover, the lower R^2 values exhibit that the pectin/PIC solutions don't follow Newtonian behaviour, which is typical for gels. The consistency index (K) and flow behaviour index (n) of the Power Law model and the Herschel-Bulkley model represent the viscosity and shear thinning/shear thickening behaviour of the fluid, respectively. K values of both the Power law and the Herschel-

Bulkley model increase with the increase in pectin/PIC solution concentration, resulting in their thicker nature. Moreover, *n* values of the Power law model are less than 1 for all samples, resulting in a decrease in viscosity with an increase in shear rate, suggesting their shear-thinning behaviour. The values of R^2 were higher when data fitted to the Power law model than compared to the Newtonian model, suggesting a better fit and, thus, more suitable to predict the flow behaviour of pectin/PIC solutions. The yield stress (T_0) in the Herschel-Bulkley model was observed for both pectin/PIC solutions, resulting in the presence of minimum stress required to disrupt the cross-linked structure and initiate the flow. Thus, pectin/PIC solutions follow the Herschel-Bulkley model with higher R^2 values.

4.3.4.3. Viscoelastic properties of PIC solutions

The dynamic frequency test was done to study the viscoelastic properties of pectin and PIC solutions at varying concentrations (1-3% w/v). The storage modulus (G′) and loss modulus (G″) were measured as a function of angular frequency. In all concentrations of pectin and PIC, the G″ was higher than G′ at low frequencies, signifying dominant viscous behaviour. With the increase in angular frequency, G′ increased compared to G″, causing crossover points. In both pectin and PIC solutions, the crossover point was shifted to a lower angular frequency with an increase in pectin and PIC concentration, as seen in Figure 4.8. This shifting of crossover points suggests that the solution behaves more elastic at lower frequencies. The stronger elastic characteristics of the solution are caused by increased network formation and molecular interactions like ionic and hydrogen bonding. As a result, G′ becomes more prominent over a wider frequency range, indicating a better-organized viscoelastic network and stronger gel-like activity in the solution. This behaviour of pectin and PIC solutions is necessary for the food industry, such as jam and jelly processing, and the pharmaceutical industry, for controlled-release drug delivery systems.

Table 4.4. The fitting parameters of the Power law, Newtonian and Herschel-Bulkley models

S.No	Models		Pectin			PIC		
			1%	2%	3%	1%	2%	3%
1	Newtonian	μ (Pa.s)	0.1198	0.2497	0.9273	0.0280	0.0520	0.0548
		R^2	0.6167	0.7464	0.8675	0.2807	-0.1555	-0.4031
		RMSE	1.5236	2.6136	7.5343	0.6245	1.0857	1.1262
2	Power law	K	0.8591	1.5310	4.3450	0.2065	0.7827	0.9163
		n	0.5164	0.5565	0.6244	0.5047	0.3219	0.2942
		R^2	0.8607	0.9480	0.9980	0.3674	0.4815	0.5243
		RMSE	0.9314	1.2003	0.9468	0.5942	0.7379	0.6653
3	Herschel Bulkley	T_0 (Pa)	1.7180	2.6700	1.7540	0.6285	1.394	1.5300
		K	0.0892	0.3395	3.5260	0.0001	0.001	0.0012
		n	0.9960	0.8274	0.6671	2.2710	1.7750	1.7200
		R^2	0.9113	0.9727	0.9985	0.6066	0.6906	0.7817
		RMSE	0.7541	0.8822	0.8211	0.4756	0.5786	0.4575

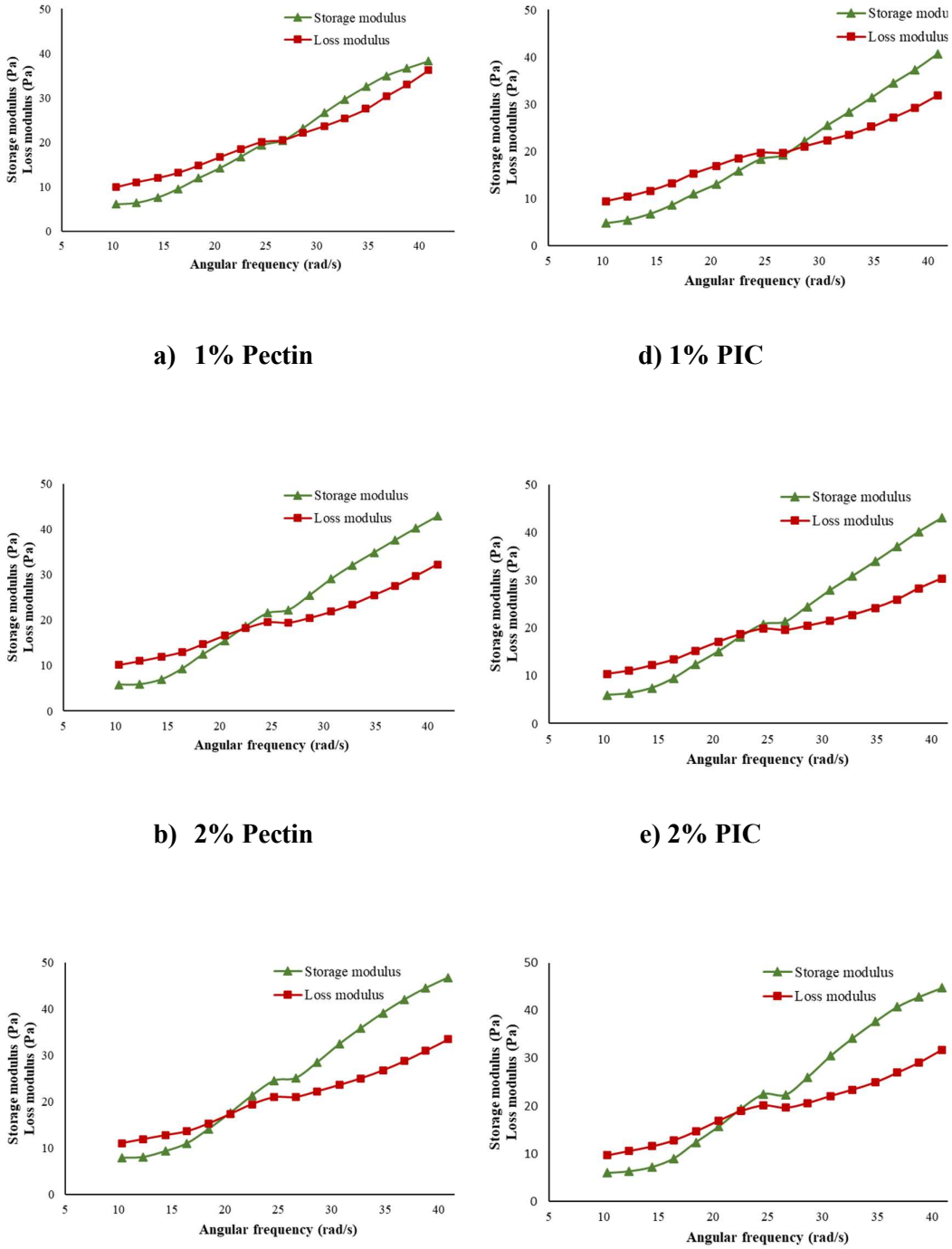

Figure 4.8. Concentration-dependent storage modulus (G′) and loss (G″) modulus profiles with respect to angular frequency (rad/s) for pectin and PIC

4.3.5. Thermal analysis of PIC in comparison with pectin

4.3.5.1. Differential Scanning Colorimetry (DSC)

The Figure 4.9. shows a DSC thermogram of pectin and PIC. The thermal curve of pectin shows two broad endothermic peaks and one exothermic peak. One of the endothermic peaks was found to be at 79.2°C having an onset at 35.8°C and end at 152.7°C with the enthalpy of fusion of 0.9047 J/g and another at 197.9°C having an onset at 183.7°C and end at 216.6°C with the enthalpy of fusion of 0.7932 J/g. The thermal curve of pectin also exhibits one sharp exothermic peak at 249.2°C with the onset at 236°C and end at 263.1°C with the enthalpy of fusion of 0.4782 J/g. Whereas the thermal curve of PIC exhibits one endothermic peak at 66.2°C having an onset at 38°C and end at 107.3°C and an exothermic peak at 256.0°C having an onset at 236.4°C and end at 275.7°C with the enthalpy of fusion of 1.527 J/g and 0.2635 J/g, respectively.

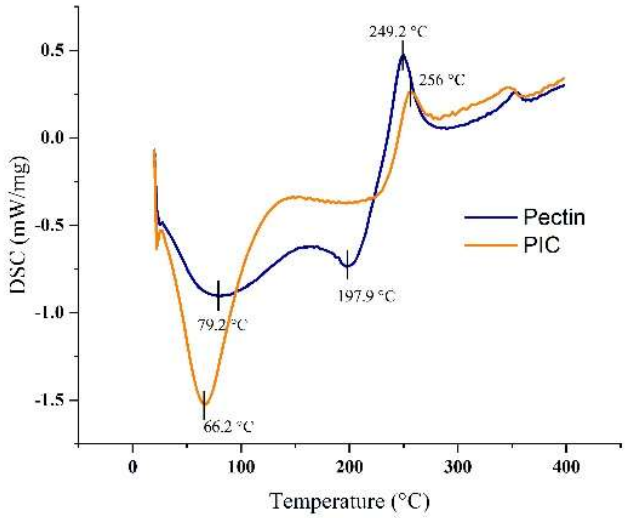

Figure 4.9. DSC of pectin and PIC

The endothermic peaks could be caused by hydrogen bonding between galacturonic acid units, the presence of water, or a conformational shift that resulted in the galacturonan ring changing from its more stable $^4C_1$ chair conformation to its inverse $^1C_4$ chair conformation (Einhorn-Stoll and Kunzek, 2009). The peak of PIC shifted somewhat toward a lower temperature, most likely as a result of its altered structure and increased water content. According to Wang et al. (2016), the exothermic peak, on the other hand, represents the

thermal degradation of the PIC and pectin samples, which is connected to their chemical ingredient profile. The exothermic peak of PIC (256.0°C) was higher than the pectin (249.2°C), indicating that PIC pectin has better thermal stability (Ezzati et al., 2020). Typically, pectin is a food ingredient that may be added to baked goods like cakes, bread, and pastries that are exposed to high temperatures (Combo et al., 2013). Furthermore, the thermal analysis in the present study revealed that PIC had greater thermal stability than pectin, suggesting that PIC can be preferable to pectin when thermal food processing is involved.

4.3.5.2.Thermogravimetric (TGA) analysis

The TGA analysis also showed three main regions at 50-200, 200-400 and 400-600°C (Fig. 4.10). A little weight loss of around 10% to 15% was seen in the first area, most likely as a result of free or absorbed water evaporating in the space between chains. Due to the pyrolytic breakdown of the PIC and pectin chains, there was a significant mass loss (roughly 50%) during the second stage (200–400°C) (Ezzati et al., 2020). First, the galacturonic acid chains underwent extensive thermal degradation. Subsequently, the acid side group and carbon in the ring underwent decarboxylation, resulting in the development of various gaseous products and the production of solid char (Wang et al., 2016).

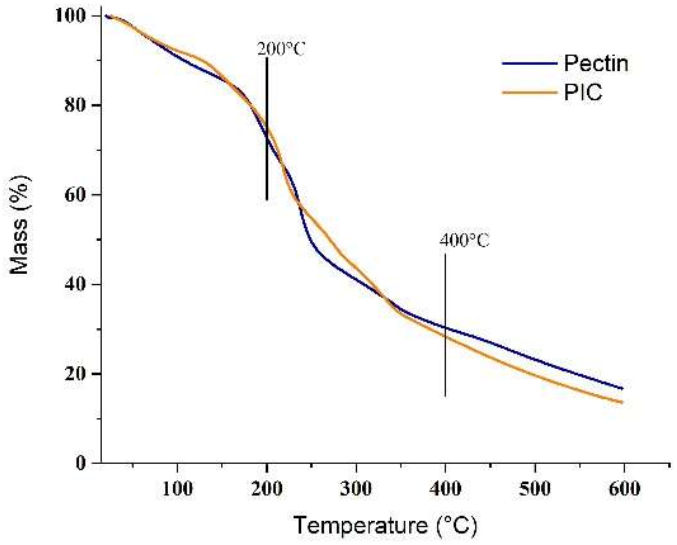

Figure 4.10. TGA of pectin and PIC

According to Ezzati et al. (2020), the third stage result revealed an additional little mass loss associated with the thermal breakdown of char. The solid char containing polyaromatic structures bonded by aliphatic and ketonic groups would partially collapse and stack compactly when the pyrolytic temperature rise (Zhou et al., 2011; Wang et al., 2016). PIC was shown to have a lower mass residue (13.50%) than pectin (16.59%), most likely as a result of PIC exhibiting a lower DE value (Ezzati et al., 2020). According to Einhorn-Stoll et al. (2007), pectin with a lower DE value has more free carboxylic groups accessible, creating more hydrogen bonds and accelerating the breakdown of pectin chains.

4.3.6. *In-vitro* iron release from PIC

The proportion of Fe remaining in the supernatant of extracted pectin and PIC after *in vitro* simulated digestion indicates the bioavailable condition of soluble Fe. This bioaccessible Fe has the potential to be absorbed by intestinal cells, increasing its bioavailability and physiological usage inside the body. It can be deduced from Figure 4.11 that the PIC's % bioaccessibility was much greater than that of extracted pectin. The total Fe content of the pectin and PIC is 23 ppm and 2657 ppm, respectively. Fe concentration in pectin is negligible after exposure to *in vitro* conditions. While, after exposure to simulated oral, gastric, and intestinal conditions, the Fe concentration in PIC is 143.978 ± 4.20, 144.235 ± 0.85, and 141.913 ± 4.20 ppm, respectively is statistically insignificant ($p<0.05$) (Figure 4.12). The concentration of Fe remained unchanged under simulated *in vitro* conditions, indicating that the structure of the PIC stayed intact even in the acidic environment of the gastric fluid. This stability might be attributed to the existence of a Fe core encased by pectin ligands (Ma et al., 2021). The bioavailability of Fe released from the selected PIC was determined to be 5.34 ± 0.16%, indicating effective absorption potential. Similar findings were seen in Gupta et al. (2006). The iron bioavailability in green leafy vegetables such as *Digera arvensis* Forsk. and *Trianthema portulacastrum* L. were 7 and 6%, respectively.

While in other green leafy vegetables in the study, iron bioavailability was found to be in the range of 16-43%, which is 3 to 8-fold of the result found in the present study (Gupta et al., 2006). Additionally, the structure of the PIC shielded the Fe ions during passage through the stomach phase, thereby mitigating potential stomach discomfort induced by the Fe ions and preserving their activity.

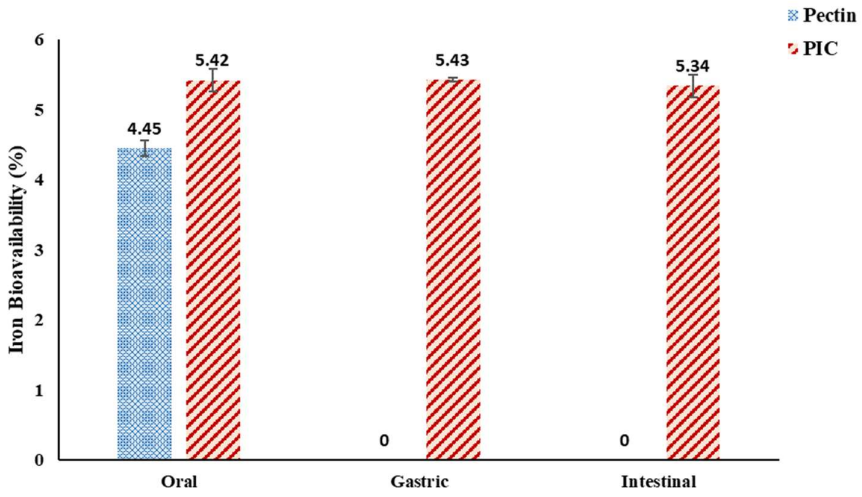

Figure 4.11. % iron bioavailability in pectin and PIC

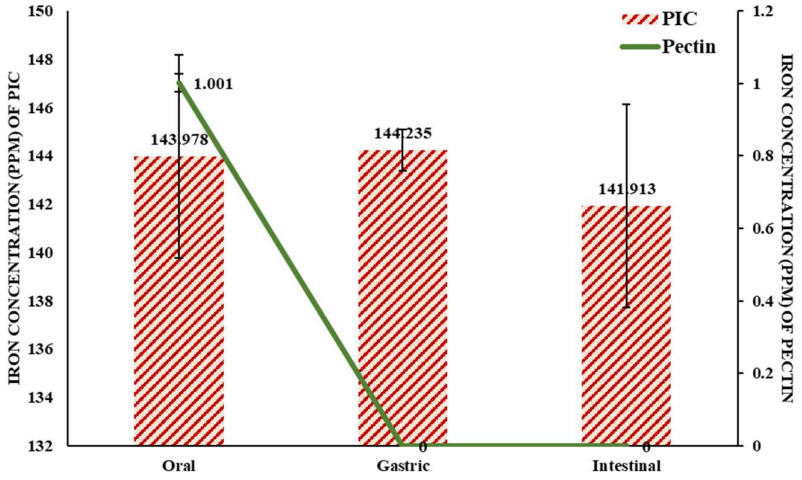

Figure 4.12. Iron concentration in pectin and PIC

Consequently, a higher concentration of Fe was transported to and accumulated in the intestinal fluid. These results highlight the possibility of PIC as a novel Fe supplement for addressing Fe deficiency in anaemic patients (Ma et al., 2021). Utilizing Fe-deficient fruits and vegetables such as cucumbers and pineapple to develop functional foods holds tremendous promise for PIC towards better nutrition.

4.3.7. Iron release study from PIC using Caco-2 cells

Caco-2 cells may differentiate to become tiny intestinal enterocytes with all the necessary Fe absorption and transport proteins; therefore, they are a well-established model for assessing non-heme Fe intake through ferritin synthesis (Eagling et al., 2014). In this study, specialized Caco-2 cells were exposed to pectin and PIC supernatants. The conversion of Fe(III) to Fe(II) has the potential to enhance Fe absorption, as Fe(II) can be efficiently conveyed through enterocytes via the divalent metal-ion transporter 1. This process facilitates the uptake of Fe by the cells, thereby contributing to its bioavailability and physiological utilization (Wang et al., 2019). The average Fe absorption was 77.807 ± 0.697 ppm, representing 2.93% of the total Fe present in PIC, while 54.82% of the overall Fe was introduced to the differentiated cells. This result is comparable with Bryszewska et al. (2019), conducting an *in-vitro* study of iron transport using Caco-2 cells from breads fortified with microencapsulated iron. In their case, the iron transport of four breads with the addition of microencapsulated iron by sourdough fermentation was in the range of 3.23-5.25% (Bryszewska et al., 2019). However, a negligible amount of Fe was present in pectin in intestinal fluid; therefore, there was no chance of Fe uptake by the differentiated Caco-2 cells. The Fe absorption values observed after 2 h of incubation remained consistent throughout the study, with no significant differences observed over time. It is well-established that under saturation conditions, Fe accumulation occurs rapidly, typically showing a sharp increase in Fe uptake within the initial 40-60 min of exposure. This phenomenon indicates the efficient uptake and accumulation of Fe by the cells under the experimental conditions. This causes the Fe concentration within the cells to plateau (Ghibaudo et al., 2018). In the brush border of enterocytes, soluble free inorganic Fe is absorbed at the gut level. While Fe(III) is absorbed through a divalent metal transporter 1 (DMT1), Fe(II) is absorbed directly. During the first reduction of Fe(III) to Fe(II), DMT1 can then transport the latter over the brush border membrane (Steele et al., 2005; Ghibaudo et al., 2018).